Received: 16 July 2020 | Revised: 13 October 2020 | Accepted: 13 October 2020

DOI: 10.1002/pc.25856

RESEARCH ARTICLE

Polymer COMPOSITES WILEY

Hybrids nanocomposites based on a polymer blend (linear low-density polyethylene/poly(ethylene-*co*-methyl acrylate) and carbonaceous fillers (graphene and carbon nanotube)

Mário A. B. S. Nunes[1] | **Bruno R. de Matos**[2] | **Glaura G. Silva**[3] | **Edson N. Ito**[4] | **Tomás J. A. de Melo**[1] | **Guilhermino J. M. Fechine**[5]

[1]Department of Materials Engineering, Federal University of Campina Grande, Campina Grande, Paraiba, Brazil

[2]Hydrogen Fuel Cells Center, Nuclear and Energy Research Institute, São Paulo, São Paulo, Brazil

[3]Center for Technology in Nanomaterials and Graphene, Federal University of Minas Gerais, Belo Horizonte, Minas Gerais, Brazil

[4]Department of Materials Engineering, Federal University of Rio Grande do Norte, Natal, Rio Grande do Norte, Brazil

[5]Mackenzie Institute for Research in Graphene and Nanotechnologies - MackGraphe, Mackenzie Presbyterian University, São Paulo, São Paulo, Brazil

Correspondence
Guilhermino J. M. Fechine, Mackenzie Institute for Research in Graphene and Nanotechnologies - MackGraphe, Mackenzie Presbyterian University, São Paulo, SP 01302-907, Brazil.
Email: guilherminojmf@mackenzie.br

Tomás J. A. de Melo, Department of Materials Engineering, Federal University of Campina Grande, Campina Grande, PB 58429-900, Brazil.
Email: tomas.jeferson@ufcg.edu.br

Funding information
Conselho Nacional de Desenvolvimento Científico e Tecnológico, Grant/Award Numbers: 306307/2019-7, 307665/2018-6; Coordenação de Aperfeiçoamento de Pessoal de Nível Superior; Fundação de Amparo à Pesquisa do Estado de São Paulo, Grant/Award Number: 2018/10910-8

Abstract

Interfacial or separate phase location of carbonaceous nanofillers (graphene and carbon nanotubes) in polymer blends with co-continuous phases can lead to double percolation behavior, significantly increasing rheological and electrical properties. The prediction of the morphology and the location of the nanofillers has been used as a tool to evaluate the proprieties of co-continuous polymer blends. This work aims to highlight the superior conductivity levels achieved using a low amount of carbon-based fillers, by the proper selection in a multiphase polymer matrix as a template for controlled dispersion and spatial distribution of the nanoparticles, offering a compromise between easy processability and enhanced performance. Here, two polymers (linear low-density polyethylene [LLDPE] and ethylene-*co*-methylacrylate [EMA]) and their co-continuous blend (LLDPE/EMA) were loaded with nanofillers (few-layer graphene [FLG], few-walled carbon nanotube [FWCNT]) via continuous melt mixing in twin-screw extrusion, separate and simultaneously. It was observed that the addition of the nanofillers changed the co-continuity of the blend, with the probable migration of the nanofillers from the EMA (hydrophilic) phase to the LLDPE (hydrophobic) phase. Rheological percolation occurred preferentially in blends containing FWCNT and FLG/FWCNT. Electrical conductivity was observed in all compositions, with higher electrical conductivity being noticed in hybrids.

KEYWORDS

conducting polymers, nanocomposites, nanotechnology, polyethylene, rheology

1 | INTRODUCTION

Conductive polymer nanocomposites (CPCs) have generated significant interest due to their range of applications, ease of manufacture, and their adjustable properties, depending on the composition and properties of the selected materials. In the development of CPCs, the use of nanoparticles, such as carbon nanotubes (CNTs) and graphene, dispersed in a polymer matrix, produces a co-support network between both fillers,[1,2] which is electrically conductive but directly dependent on the properties of the polymer and filler used. To produce conductive nanocomposites, the excellent electrical properties of the graphene and CNT cannot be disturbed by the formation of agglomerates to obtain nanocomposites with satisfactory electrical conductivity.

The performance of CPCs is not only achieved using nanofillers with excellent conducting properties, but by also optimizing the dispersion, interfacial chemistry, and nanoscale morphology to take advantage of the large surface area per unit of volume that they present. Considering the high surface area of the nanoparticles and the dispersion, their application in CPCs at low volumetric fractions can generate a co-continuous network of particles,[3] and affect the behavior of the surrounding polymer matrix,[4,5] leading to a modification of its thermal, mechanical, and electrical properties.

A highly conductive co-continuous network can be obtained using high aspect ratio fillers, allowing the achievement of an equal or greater electrical conductivity observed in a conductive nanocomposite with lower filler content compared to one with high filler content. However, to achieve a better balance between electrical conductivity and mechanical properties, the formation of a structure with double percolation is essential. This kind of structure, typical of a polymer blend with co-continuous morphology, can induce the conductive fillers to be selectively located in one of the phases or at the interface between them, significantly reducing the amount of filler necessary to build an electrical percolated network.[6]

Bai et al[7] demonstrated recently that the interfacial location of graphene in polymer blends with co-continuous phases proved to be effective in stabilizing the morphology and increasing conductivity with a low electrical percolation threshold. In this work, blends of polylactic acid (PLA) and polystyrene were obtained with thermally reduced graphene oxide (r-GO) located on the interface. The resulting nanocomposites showed significantly higher conductivity at low filler fractions, having a percolation threshold of about 0.028% by volume. It has also been found that r-GO is transferred from the PLA phase to the interface during mixing and annealing, giving rise to a 3D network, which stabilizes the co-continuous structure. It was concluded that the premixing process, as well as, the blending sequence were determining factors for the r-GO particles' location in the blend.

Al-Saleh[8] investigated the electrical properties of nanocomposites mixed by melting graphene nanoplatelets/polypropylene (GNPs/PP) and also with GNPs/CNT/PP. The influence of the processing conditions on the electrical properties of the prepared nanocomposites was evaluated. It was also found that the electrical percolation threshold of the GNPs/PP nanocomposite was 4 vol% and that after adding only 1% by weight of CNT in the GNPs/PP blend, a significant improvement in electrical properties was obtained. However, the CNT/PP nanocomposite exhibited better conductivity compared to the GNPs/PP and GNPs/CNT/PP nanocomposites. For the same concentration of nanofillers, the GNPs/CNT/PP hybrids showed better properties with the increase in the CNT volume fraction due to the better dispersion of the nanotubes and their strong adhesion at the CNT/PP interfaces.

It has been demonstrated that nanocomposites containing two immiscible polymers, where one of the phases is an amorphous or a semicrystalline polymer matrix, and the other is an elastomer, can reduce the percolation threshold through the formation of a more extensive conductor network.[9–11] Although there are many studies involving carbon-based conductive nanocomposites, the vast majority make use of multilayered CNTs (MWCNTs) and GNPs. However, it is known that few-walled CNTs (FWCNTs) stand out from other types of nanotubes as they retain the mechanical and electronic properties of the inner layers.[12] Few-layer graphene (FLG) is better than GNPs for electronic applications because, as shown by Fang et al,[13] the electrical conductivity of graphene is considerably reduced with the increase in the number of layers.

Although there is already a study of an linear low-density polyethylene/ethylene-*co*-methylacrylate (LLDPE/EMA) blend, neither this study nor those that evaluated other similar polymer nanocomposites containing carbonaceous nanofillers, made use of FLG and FWCNTs under the conditions herein. The influence of two different nanofillers (FLG and FWCNT) and the mixture strategy on the structural and electrical properties of nanocomposites based on LLDPE, EMA, and LLDPE/EMA as matrices were investigated. Fourteen compositions (four with LLDPE, four with EMA, and four with LLDPE/EMA blend) with varying nanofiller contents (1.5 and 3 wt% of FLG; 1 and 2 wt% of FWCNT) and two hybrids with LLDPE/EMA (1.5%FLG/1%FWCNT and 3FLG%/2%FWCNT) were prepared, using the solid-solid deposition (SSD) method[14] in a twin-screw extruder.

The motivation of the present work is to highlight the superior conductivity levels achieved using a lower amount of carbon-based fillers when compared with other studies, by the proper selection in a multiphase polymer matrix as a template for controlled dispersion and spatial distribution of the nanoparticles, offering a compromise between easy processability and enhanced performance. The influence of different mixing strategies on the molten state and the different formulations, as well as the reflection of these variables, were evaluated through analysis of the surface (contact angle [CA]), structural (Raman spectroscopy), morphological (scanning electron microscopy [SEM]), rheological (oscillatory tests), and electrical properties of the carbon-based nanocomposites.

2 | MATERIALS

In this work, LLDPE (SLL318, Braskem) with a melt flow index of 2.7 and a processing temperature range between 170°C and 210°C, and EMA (Arkema) with a melt flow index of 2 to 3.5 g/10 minutes and a melting peak of 61°C were used as received (pellets). Graphene with an average specific area of 137.3 m^2/g and a lateral size of 1 μm was purchased from 2DM Materials (Singapore). CNTs with a diameter distribution of 3 to 9 nm, a length of 100 to 200 μm, and a purity of 90% were donated by CTNANO/UFMG (Brazil). The compositions were designated from the abbreviations of each component (FLG, FWCNT, EMA, and LLDPE), with the different mass fraction values of the fillers (x and y), located in front of each name (xFLG and yFWCNT). For the LLDPE/EMA composition, the blend abbreviation was chosen, hiding the fraction of each polymer (60% of LLDPE and 40% of EMA) since it was the only blend composition used, as shown in Table 1.

3 | METHODOLOGY

3.1 | Preparation of CPC films

For the manufacture of the nanocomposites, a corotational twin-screw extruder $L/D = 40$ (Process 11, ThermoScientific) was used, adopting a feeding rate of 4 g/min, a profile temperature from the funnel up to the die of 170°C/170°C/180°C/180°C/190°C/190°C/200°C/200°C, and a screw speed of 150 rpm. The impregnation of the polymer matrices was completed using the SSD method,[14] where the ground polymer (LLDPE or EMA), the nanofiller (FLG, FWCT, or FLG/FWCNT),

TABLE 1 Compositions with respective fractions of each component used

		Mass fraction (wt%)			
N	**Abbreviation**	**LLDPE**	**EMA**	**FLG**	**FWCNT**
1	LLDPE	100		—	—
2	EMA	—	100	—	—
3	Blend	60	40	—	—
4	LLDPE/1.5%FLG	100	—	1.5	—
5	EMA/1.5%FLG	—	100	1.5	—
6	LLDPE/3%FLG	100	—	3.0	—
7	EMA/3%FLG		100	3.0	—
8	LLDPE/1%FWCNT	100	—	—	1.0
9	EMA/1%FWCNT	—	100	—	1.0
10	LLDPE/2%FWCNT	100	—	—	2.0
11	EMA/2%FWCNT	—	100	—	2.0
12	Blend/1.5%FLG	60	40	1.5	—
13	Blend/3%FLG	60	40	3.0	—
14	Blend/1%FWCNT	60	40	—	1.0
15	Blend/2%FWCNT	60	40	—	2.0
16	Blend/1.5%FLG/1%FWCNT	60	40	1.5	1.0
17	Blend/3%FLG/2%FWCNT	60	40	3.0	2.0

Abbreviations: EMA, ethylene-*co*-methylacrylate; FLG, few-layer graphene; FWCNT, few-walled carbon nanotube; LLDPE, linear low-density polyethylene.

and the water solution (containing the exfoliated graphene sheets) are added to a round-bottom flask. While the mixture is drying, the rotational movement of the rotoevaporator makes it possible to impregnate the granulated polymer with the nanoparticles. In the compositions containing only FWCNT, the direct addition of these fillers occurred during mixing in an R-100 Rotavapor from Buchi.

For the compositions containing FLG/FWCNT or FLG, water exfoliation was performed in an ultrasonic bath (Elmasonic P 60H) for 2 hours at T_{amb}, before the impregnation process. After the rotoevaporation, the polymers impregnated with the nanofillers were dried in a vacuum oven for 14 hours at 50°C. After that, all the compositions containing one polymeric matrix underwent one extrusion step. It is vital to remember, for the compositions containing two matrices, that the impregnation took place in only the EMA matrix, where after the first extrusion step, a second extrusion was performed when the LLDPE matrix was added. The extruded material was then milled, and compression-pressed films were prepared in a Solab uniaxial hydraulic press, with a capacity of 15 T, at a temperature of 170°C, according to the following pressurizing ramp: 0.5 T for 1 minute and 30 seconds, followed by the application of 2 T for 2 minutes. The pressed films were then removed from the press and placed on a flat, cool surface, and allowed to cool in air. The evaluated compositions with their respective fractions of each component are described in Table 1. Here, is important to mentioned that the fillers concentrations were chosen with values below those found in the literature (10-20 wt%[8,15–17]) applying a processing methodology developed by our research group[14] in order to achieve better conductivity values.

4 | CHARACTERISATIONS

4.1 | Surface properties analysis

The wettability of the polymeric films was evaluated using a KRÜSS goniometer—Drop Shape Analyzer (DSA100) based on the sessile drop method. All the tests were carried out in an air atmosphere at 20°C using deionized water (γ = 72.1 mJ/m^2, γ^p = 51 mJ/m^2 and γ^d = 21.8 mJ/m^2) and ethylene glycol (γ = 47.7 mJ/m^2, γ^p = 21.3 mJ/m^2 and γ^d = 26.4 mJ/m^2) as wetting solvents. The surface energy, dispersion, and polar components were estimated using the Owens-Wendt-Rabel-Kaelble method[18,19] which is a modification of the Fowkes model[20] and calculated as follows:

$$\gamma_{SV} = \gamma_{SV}^d + \gamma_{SV}^p \quad (1)$$

$$\gamma_{LV} = \gamma_{LV}^d + \gamma_{LV}^p \quad (2)$$

$$\gamma_{SL} = \gamma_{SV} + \gamma_{LV} - 2\sqrt{\gamma_{SV}^d \cdot \gamma_{LV}^d} - 2\sqrt{\gamma_{SV}^p \cdot \gamma_{LV}^p} \quad (3)$$

$$\gamma_{LV}(1 + \cos\theta) = 2\sqrt{\gamma_{SV}^d \cdot \gamma_{LV}^d} + 2\sqrt{\gamma_{SV}^p \cdot \gamma_{LV}^p} \quad (4)$$

where θ is the CA of the liquid, γ_{SV} is the solid surface tension, γ_{LV} is the liquid surface tension, γ_{SL} is the liquid-solid interfacial tension, and $\gamma_{SV}^d, \gamma_{SV}^p, \gamma_{LV}^d, \gamma_{LV}^p$ represent the contributions from the dispersion and dipole-dipole interaction of γ_{SL} and γ_{LV}.[21] All the measurements were performed at least 5 times for each drop evaluated; the mean and SD were taken from 50 CA measurements from the same drop.

4.2 | Raman spectroscopy

Raman spectra of the polymeric films were obtained using a WITEC Raman spectrometer, model UHTS 300, coupled to a Witec CCD detector (model DV401A-BV-352). The focusing of the laser on the sample and the collection of scattered radiation were completed using a Witec optical microscope (Carl Zeiss, Serien-Nr 334000409). An excitation line with a wavelength at 532 nm of an Nd-YAG laser (Photonics, model Xtra-OS-00400), 10 accumulations, 4 seconds/spectrum integration time, and ×100 magnification lens was used. The integrity and quality of the FLGs and FWCNTs nanofillers were evaluated after melt blending, and the interfacial interactions between the polymers and the CNTs were investigated.

4.3 | Scanning electron microscopy

The morphologies of the samples were analyzed using a field emission gun SEM (SEM, Auriga, Zeiss), with a voltage of 5 kV. Before SEM analysis, LLDPE/EMA nanocomposites were fractured in liquid nitrogen and sputtered with a thin layer of gold using a sputtering machine (Bal-Tec SCD).

4.4 | Rheological analysis

Rheological measurements were made at 200°C in an Anton Paar rotational rheometer, model Physica MCR

301, which is equipped with a parallel plate of $\Phi_{25\ mm}$ and a gap of 1 mm. The sample chamber was purged with continuous airflow. A strain amplitude of 1% was applied for the oscillatory frequency sweep of 0.1 to 625 rad/s. The influence of the dispersion degree on the electrical conductivity of the nanocomposites was evaluated.

4.5 | Electrical conductivity

Electrical conductivity was measured at room temperature using a Solartron, model 1260A, impedance analyzer, where the polymeric films were placed between two carbon cloth electrodes (area of 0.785 cm^2) coated with a Teflon/Vulcan carbon ink to ensure good contact and minimizing sample/electrode interfacial impedance. For each conductivity value obtained, three measurements were made on three different samples. The impedance spectra were collected at the frequency range of 0.1 Hz to 1 MHz, and the electrical conductivity (σ) was obtained from Equation (5):

$$\sigma = \frac{1}{\rho} = \frac{d}{RS} \tag{5}$$

where ρ is the electrical resistivity, d is the thickness of the samples, and S is the cross-sectional area. The electrical resistance R was obtained from the intercept of the low-frequency limit of the impedance arc with the real axis of the complex plane.

5 | RESULTS

5.1 | Prediction of co-continuous morphology of polymer blends

It is known that the development of the morphology depends on the rheological properties of the components of the blends, interfacial tension, the composition of the blends, and the processing conditions.[22] As blends with co-continuous morphology may offer more interesting combinations of properties than blends with a dispersed-type structure, there has been a growing interest in this type of material.[23] For example, a co-continuous structure significantly improved the electrical properties of conductive polymeric nanocomposites, in comparison with the same blends with a dispersed morphology.[6,24,25]

When developing co-continuous structures by the intensive mixing of two melted polymers in a shear field, the blend becomes more effective when the viscosities and volume fractions of the two components are the same. This happens because equal volume fractions maximize the opportunity to maintain connectivity, as no component is present in a smaller quantity. Nevertheless, in most systems, the viscosities of the components are different.[26]

The following relationship describes the phase inversion composition in terms of volume fractions and viscosity.

$$\phi_{1,PI}/\phi_{2,PI}{}^{*}\eta_2/\eta_1 \cong 1 \tag{6}$$

where η_i is the viscosity and $\phi_{i,PI}$ is the volumetric fraction of the phase inversion of component i. Using $\lambda = \eta_2/\eta_1$ and $\phi_{1,PI} = 1 - \phi_{2,PI}$, the phase inversion composition becomes:

$$\phi_{2,PI} = \frac{1}{(1+\lambda)} \tag{7}$$

The relationship represented by Equations (6) and (7), proposed by Utracki, is not sufficient to make this prediction since one of the conditions that must be satisfied for its use is that the viscosity ratio between the polymers must be equal to 1.[27–29]

Utracki[28] subsequently developed an approach based on "intrinsic viscosities" $[\eta]$ and the maximum volumetric fraction of packaging $\emptyset_m$, including the viscosity concentration behavior and assuming that the viscosities of the blend resulting from the addition of polymer 2 to polymer 1 and vice versa are the same in the phase inversion composition. Using this argument and a relation given by Krieger and Dougherty to rigid monodispersed spheres, he developed Equation (8), which can be simplified for the relation given in Equation (9), for values of λ between 0.1 and 10.

$$\lambda = \left[\frac{\phi_m - \phi_{2,PI}}{\phi_m - \phi_{1,PI}}\right]^{[\eta]\emptyset_m} \tag{8}$$

$$\phi_{2,PI} = \frac{(1 - log\lambda/[\eta])}{2} \tag{9}$$

Assuming that $[\eta]$ is equal to 1.9 for spherical domains and that $\phi_m = 0.84$.

With this knowledge in mind, the starting point is the calculation of the phase inversion composition $Ø_{PI}$ where theoretically co-continuity can be found. For this, it is necessary to initially calculate the shear rate (γ) in the screw channel,[30] because from this value the viscosity values of the polymers that need to be used in Equation (10) are known.

$$\gamma = \frac{\pi x D x N}{h} \quad (10)$$

where γ (s^{-1}) is the approximated shear rate in the screw channel, D (mm) is the screw diameter = 11 mm, N (rps) is the screw velocity = 2.5 rps, and h (mm) is the channel depth = 0.2 mm.

With the value of each variable, as showed below, we applied Equation (10) again:

$$\gamma = \frac{\pi x D x N}{h} = \frac{\pi x 11 x 2.5}{0.2} = 431.96\,\mathrm{s}^{-1}$$

After obtaining the shear rate, capillary rheology was performed on a Ceast, model SR20, capillary rheometer on the LLDPE and EMA matrices to obtain the viscosity values required for the calculation of the λ viscosity ratio as described by Equation (8).

Knowing that $\lambda = \frac{\eta_2}{\eta_1}$, as described by Equations (6) and (7).where η_1 = 778.08 Pa.s = viscosity of LLDPE and η_2 = 382.95 Pa.s = viscosity of EMA.

This gives:

$$\lambda = \frac{\eta_2}{\eta_1} = \frac{382.95\,\mathrm{Pa.s}}{778.08\,\mathrm{Pa.s}} = 0.4921$$

With the value of λ and using Equation (9):
$\phi_{2,\mathrm{PI}} = \frac{(1-\log\lambda/[\eta])}{2} = \frac{(1-\log(0.4921)/1.9)}{2} = 0.3441$ or 34.41% of EMA and $\phi_{1,\mathrm{PI}} = 1 - \phi_{2,\mathrm{PI}} = 1 - 0.3442 = 0.6559$ or 65.59 % of LLDPE.

For a screw speed of 150 rpm, and based on the calculation for the phase inversion proposed by Utracki (Equation (9)), a co-continuous morphology is predicted for the LLDPE/EMA blend when mass percentages used are close to 65% of LLDPE and 34% of EMA, as shown in Figure 1.

5.2 | CA measurements

Previous results have demonstrated that the presence of graphene and graphene oxide can modify the surface characteristics of polymer-based nanocomposites.[31,32] When the nanofiller is very well dispersed in the polymer matrix, its hydrophobic or hydrophilic character can be assessed, and modifications of the surface properties of the polymer are observed. However, if filler agglomerates are generated during the mixing process, their effect on the surface properties is suppressed.[33]

To analyze the nanocomposites' hydrophobicity, the CA (θ) of the water and ethylene glycol drops were measured over the surface of the FLG and FWCNT nanocomposites (Figure 2). It is important to know that the classifications of materials as a function of their hydrophilicity and hydrophobicity are: a superhydrophilic material when $0 > \theta_{\mathrm{water}} < 10°$; a hydrophilic material when $10° > \theta_{\mathrm{water}} < 90°$; a hydrophobic material when $90° > \theta_{\mathrm{water}} > 150°$, and a superhydrophobic material when $\theta_{\mathrm{water}} > 150°$C.[34]

The wettability of the samples with water showed an increase in the hydrophobic characteristic of the polymers when evaluated. This is due to the presence of graphene and CNTs, which are hydrophobic materials and lack polarity in carbon atoms.[35] However, the nanocomposites containing EMA retained their predominantly hydrophilic behavior because of the ester group in its molecular structure; the filler amount is not enough to change this behavior significantly. For the blends, only two compositions presented a significant influence of the

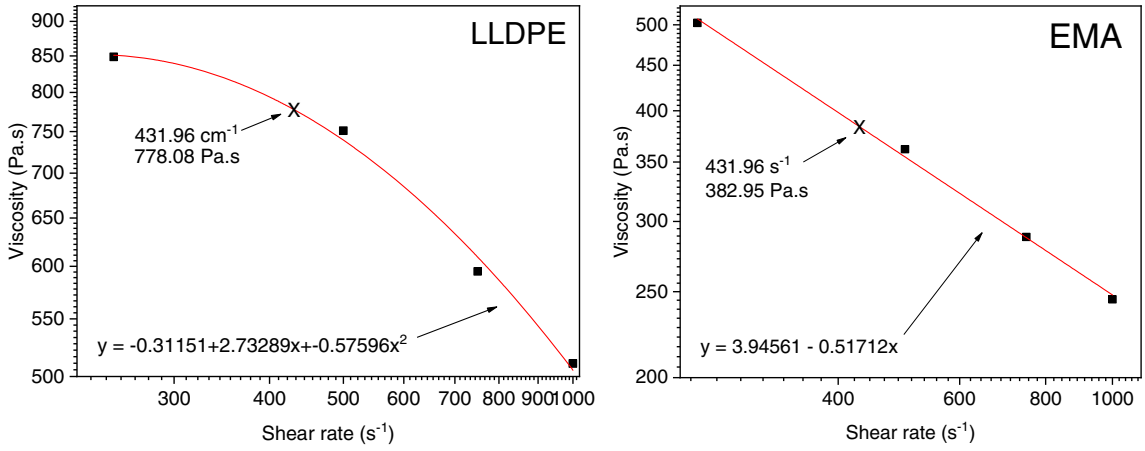

FIGURE 1 Curves of viscosity vs the shear rate of the, A, linear low-density polyethylene (LLDPE) and B, ethylene-*co*-methylacrylate (EMA) polymers [Color figure can be viewed at wileyonlinelibrary.com]

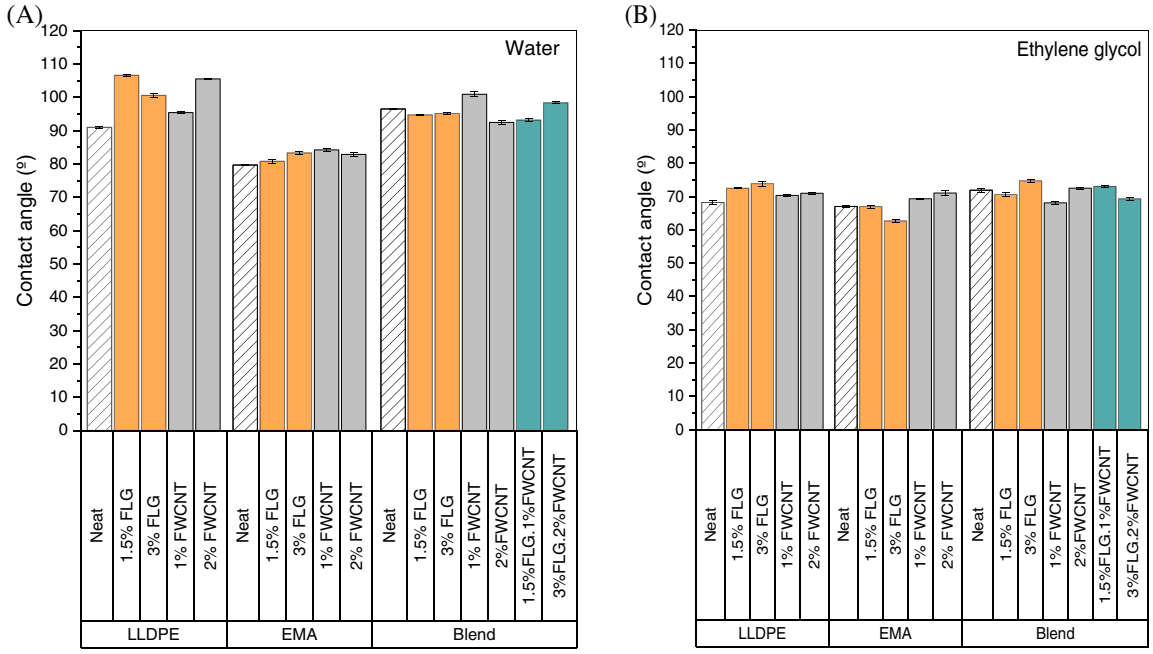

FIGURE 2 Contact angle measurements for all compositions with, A, water and, B, ethylene glycol [Color figure can be viewed at wileyonlinelibrary.com]

nanofillers on the wettability; the other compositions were not significantly affected.

Regarding the type of solvent used, the observed CA values were higher when water was used instead of ethylene glycol. This shows that charge interactions between the polymer surfaces and the nonpolar liquid are stronger than those with a polar liquid.

Polar and dispersive components of the surface energy of the carbon-based nanocomposites were analyzed, shown in Figure 3. It is known that the dispersive component of the surface energy is due to electronic interactions as "van der Waals" forces[36] and the polar component is related to the surface functional groups, that is, hydroxyl, carbonyl, carboxyl, and ether groups.[33]

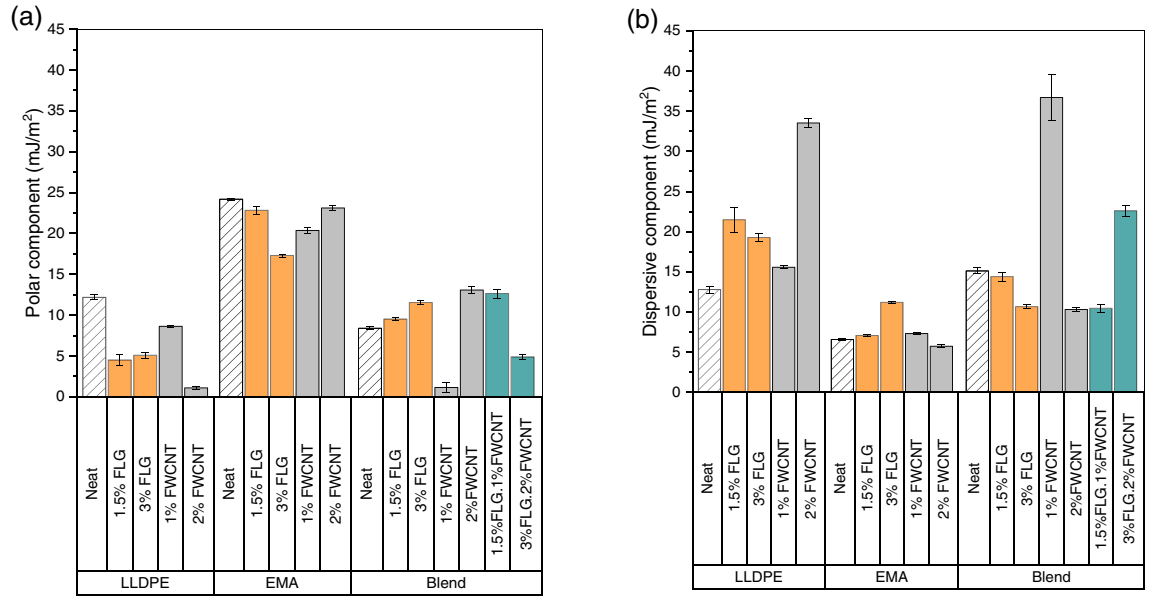

FIGURE 3 A, Polar component (γ_p) and B, dispersive component (γ_d) as a function of composition [Color figure can be viewed at wileyonlinelibrary.com]

An increase in the dispersive component of the surface energy of the LLDPE and LLDPE/EMA compositions can be observed, which is correlated with a decrease in the CA between these nanocomposites and ethylene glycol in comparison with water CA values, due to the predominantly nonpolar characteristic of the nanofillers and LLDPE. The higher values of the polar component indicate the influence of the hydrophilic characteristic attributed to the EMA nanocomposites surface, as previously shown by CA measurements.

5.3 | Raman spectroscopy

Raman spectra of graphite, FLG, and FWCNT, and the wavenumbers of the D, G, and 2D bands of the nanocomposites with EMA and LLDPE are shown in Figure 4 and Table 2, respectively. Raman spectroscopy is mainly used to characterize the three characteristic bands of carbonaceous material: the D, G, and 2D bands being centered at 1348, ~1580, and ~2693 cm^{-1} for FLG and ~1339, ~1587, and ~2665 cm^{-1} for FWCNT as shown in Table 2. The D band represents defects and structural disorder in the carbon lattice and results from the conversion of sp^2 hybridized carbon atoms into sp^3 hybridized carbon atoms.[37] In CNTs, the G band is associated with the longitudinal and transverse vibrations of the nanotubes[38]; for graphene, the G band is generally attributed to the elongation movement in the bonding plane of sp^2 carbon atoms.[39] The 2D band is the second-order band of the D band,[40] an indicator of the number of graphene layers.[41] When there is an increase in its intensity and position displacement to smaller wavelengths, this is an indication of an increase in the number of graphene layers. The intensity ratio between the D and G (I_D/I_G) bands indicates the level of defects in the graphitic structure as vacancies, heptagon-pentagon pairs, folds, and heteroatoms.[42]

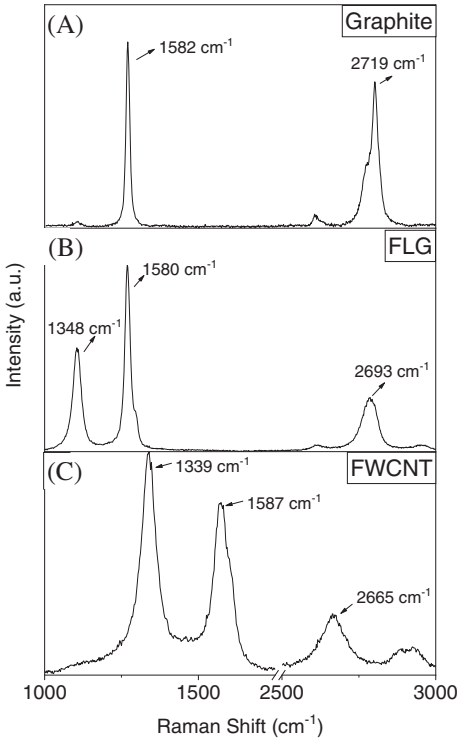

FIGURE 4 Raman spectra of, A, graphite, B, few-layer graphene (FLG), and C, few-walled carbon nanotube (FWCNT) powder

In the graphene Raman spectrum, an intense D-band and a shifted 2D-band compared to a typical graphite sample can be observed in Figure 4A,B, respectively. The D band presented in the FLG spectrum indicates that the liquid phase exfoliation step induced damage to the graphitic material edges; however, this could lead to a decrease in stacked sheets. This material was later evaluated through a G-protocol.[43] The results obtained from this analysis indicate that the acquired graphene is with a low number of stacked layers, predominantly up to five layers (Figure 5).

The D, G, and 2D bands appearing in the Raman spectrum for the LLDPE, EMA, and LLDPE/EMA nanocomposites are derived from the D, G, and 2D bands of the FWCNT and FLG, respectively. The D, G, and 2D bands of almost all evaluated nanocomposites shifted after their insertion into the different polymer matrices. This shifting to higher wavenumbers may indicate the formation of noncovalent interactions between the polymer matrices and nanoparticles.[44]

It is known that the position of the 2D band is sensitive to stress in the nanotubes, that when this band shifts up or down, there is an insertion of compressive strain or tensile strain in the CNT, respectively.[45–47] For the compositions, Blend/1%FWCNT, Blend/2%FWCNT, and Blend/1%FLG/2%FWCNT, shown in Table 2, the 2D band moved to higher wavenumbers, as a result of the intercalated polymer in the CNT bundles, which led to the insertion of compressive strain in the CNTs.

The calculated I_D/I_G intensity ratios for the FLG and FWCNT nanoparticles present in the nanocomposites were used to estimate the defect density of the nanotubes and graphene as a consequence of the melt mixing using different blending sequences as shown in Table 2. The I_D/I_G values for the FWCNT and FLG nanofillers as received were 0.989 and 0.549, respectively. It was observed that for the FLG and FWCNT nanocomposites, their value was reduced from ~0.549 to ~0.460 and from ~960 to ~901, respectively. This behavior denotes a low quantity of defects and maintenance of the structural

TABLE 2 Wavenumbers of D, G, and 2D bands with their respective I_D/I_G and I_{2D}/I_G values

Compositions		Band (cm^{-1})				
		D	G	2D	I_D/I_G	I_{2D}/I_G
FLG		1348	1580	2693	0.549	0.287
FWCNT		1339	1573	2665	0.989	0.273
LLDPE	1.5%FLG	1353 ↑	1587 ↑	2708 ↑	0.489 ↓	0.412 ↑
	3%FLG	1351 ↑	1587 ↑	2714 ↑	0.459 ↓	0.544 ↑
EMA	1.5%FLG	1353 ↑	1588 ↑	2705 ↑	0.869 ↑	0.452 ↑
	3%FLG	1352 ↑	1586 ↑	2711 ↑	0.511 ↓	0.555 ↑
LLDPE	1%FWCNT	—	—	—	—	—
	2%FWCNT	1351 ↑	1597 ↑	2706 ↑	0.922 ↓	0.616 ↑
EMA	1%FWCNT	1349 ↑	1593↑	2699 ↑	0.962 ↓	0.526 ↑
	2%FWCNT	1351 ↑	1596↑	2703 ↑	0.901 ↓	0.604 ↑
Blend	1.5%FLG	1352 ↑	1586 ↑	2713 ↑	0.464 ↓	0.496 ↑
	3%FLG	1354 ↑	1588 ↑	2710 ↑	0.539 ↓	0.474 ↑
Blend	1%FWCNT	—	—	—	—	—
	2%FWCNT	—	—	—	—	—
Blend	1%FLG	—	—	—	—	—
	2%FWCNT	—	—	—	—	—
Blend	1%FLG	1356 ↑	1588 ↑	2703 ↑	0.728 ↑	0.387 ↑
	2%FWCNT	1351 ↑	1596 ↑	2702 ↑	0.969 ↓	0.718 ↑

Note: Superior value ↑ or inferior ↓ to that observed in the FLG or FWCNT nanofillers. Raman spectra of the compositions LLDPE/1%FWCNT, LLDPE/EMA/1%FWCNT, LLDPE/EMA/2% FWCNT, LLDPE/EMA/0.5%FLG/1%FWCNT were not localized.

Abbreviations: EMA, ethylene-*co*-methylacrylate; FLG, few-layer graphene; FWCNT, few-walled carbon nanotube; LLDPE, linear low-density polyethylene.

quality of these carbon nanoparticles, even after the extrusion process. The I_{2D}/I_G ratio of FLG nanocomposites was much higher than that observed for the FLG nanofiller (an increase of about 52%), suggesting that there was a reduction in the number of layers (Figure 7C). It is known that the intensity of the 2D band, for the CNTs, is highly sensitive to tube diameter distribution and structural variations along the tube axis.[47] Therefore, the analysis of the I_{2D}/I_G intensity ratio values of the FWCNT inside the nanocomposites showed a small decrease in its values, suggesting that most of the CNT crystalline structure was preserved.

5.4 | Morphological analysis

Analysis of the micrography shown in Figure 6A,B, confirms the formation of a co-continuous morphology in the LLDPE/EMA blend as previously predicted by the calculation of the phase inversion above, based on the approach proposed by Utracki.[28]

The changes in the phase morphology of the blends typically depend on the concentration, shape, type, and dimensions of the filler. It is widely known that selective localization of the filler in binary blends typically depends on various factors like thermodynamic, kinetic, and melt viscosity of the components.[48,49] Observation of the surface fracture of the Blend/3%FLG/2%FWCNT (Figure 6D,E) composition showed that the nanofillers presence in the hybrid led to the disruption of the co-continuous morphology, leading to the migration of the nanofillers from the EMA phase, possibly to the LLDPE phase. Figure 6D,E suggests a preferential migration to LLDPE phase, since FWCNT are embedded in this matrix. Although the location of the FLG nanoparticles has not been precisely located in the presented micrographs, the rheological percolation results (Figure 7) suggest that FLG nanoparticles are supposed to be embedded in the LLDPE phase. One explanation for this behavior is that the surface interaction of systems with a higher LLDPE fraction is predominantly hydrophobic when compared to systems containing only EMA (Figures 2 and 3).

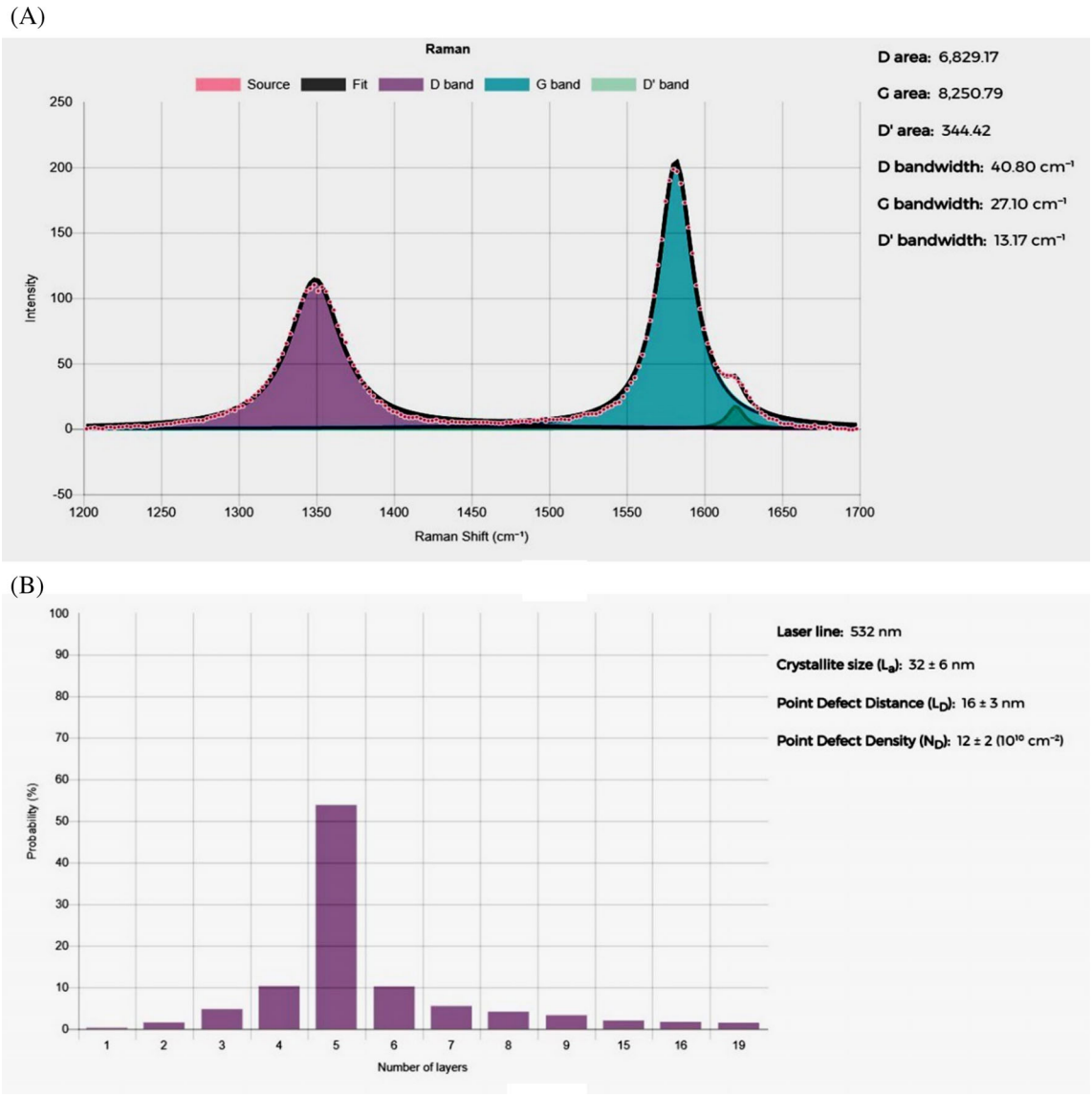

FIGURE 5 Raman analysis results of graphene powder evaluated through a G-protocol [43]. A, Lorentzian adjustment of the D, G, and D′ bands and, B, histogram with the distribution of the number of graphene layers [Color figure can be viewed at wileyonlinelibrary.com]

5.5 | Rheology analysis

Figure 7 shows storage modulus (G'), loss modulus (G''), complex viscosity ($|n^*|$), damping factor (ζ), and relaxation time (λ) as a function of frequency, and phase angle (δ) as a function of complex modulus, under an amplitude oscillatory shear (strain $\gamma = 1\%$) for a frequency range from 0.1 to 625 rad/s at 200°C. Next to each graph in Figure 7, a bar graph was placed showing the trends observed in the low angular frequency region (0.1-0.14 rad/s), which was evaluated for Figure 7A-C by the calculation of the slope straight line, and for Figure 7D-F, by the observation of the low angular values of damping factor ($\tan \delta = G''/G'$), phase angle, and relaxation time, respectively. From Figure 7A, it can be observed that at low frequencies, the storage modulus (G') and loss modulus (G'') of all nanocomposites were enhanced with higher filler concentrations. This increase is more significant with the blends containing FWCNT and FLG/FWCNT, due to the better dispersion of CNTs, as shown in Figure 6E. Figure 7C showed the same enhancement trend in the complex viscosity with the increase of the filler amount, which was more pronounced in the compositions containing CNTs, because of its high aspect ratio, which could lead to the formation of a more percolated structure in the nanocomposites.[16,50]

The liquid-solid transition point, as a result of the FWCNT and FLG network generation, cannot be easily predicted from the storage modulus or complex viscosity concerning frequency due to the elastic nature of the

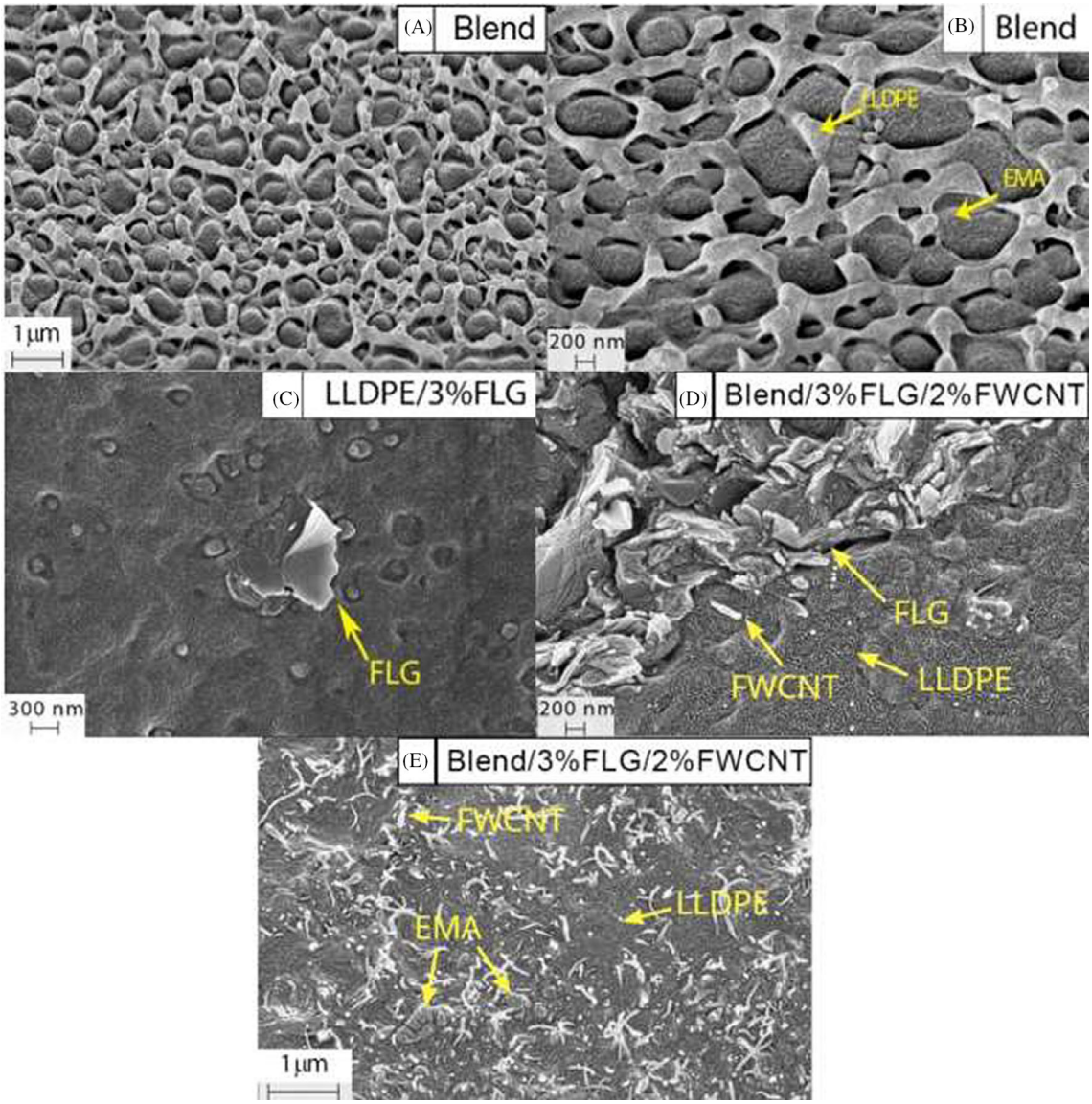

FIGURE 6 Scanning electron microscopy (SEM) micrographs of linear low-density polyethylene (LLDPE)/ethylene-*co*-methylacrylate (EMA) blend (A and B) and carbon-based nanocomposites (C-E) [Color figure can be viewed at wileyonlinelibrary.com]

polymers evaluated. Therefore, the variation of phase angle (δ) as a function of complex modulus (Figure 7E), and the damping factor ($\tan \delta = G''/G'$) with respect to angular frequency (Figure 7D) were used to estimate viscous to elastic behavior transition. It is known that when polymer chains are relaxed, the value of δ is 90° in the low G^* region.[51] With the formation of a percolated network, the phase angle is reduced to values below 45°, indicating the predominance of an elastic component over the entire frequency range.[52] Concerning $\tan \delta = G''/G'$, it is known that the closer its value is to 1, a more solid-like behavior the material will present, ($\tan \delta < 1$) and that the further from 1 ($\tan \delta > 1$), a more liquid-like behavior.[53] Although almost all the compositions presented a reduction in their values of δ and $\tan \delta$ with the increase in filler loading, it can be observed that only five compositions (LLDPE/2%FWCNT, Blend/1%FWCNT, Blend/2%FWCNT, Blend/1.5%FLG/1%FWCNT, and Blend/3%FLG/2%FWCNT) presented a predominantly elastic behavior ($\delta < 45°$ and $\tan \delta < 1$), suggesting that the network of CNTs was better developed in the LLDPE matrix and blend. For the other compositions with $\delta > 45°$ and $\tan \delta > 1$, it can be said that, despite the reductions observed in their δ e $\tan \delta$ values, some factors, such as the partial dispersion of particles, the possible presence of some agglomerates and the reduced filler quantity used may have been the contributing factor that makes a liquid-solid transition impossible for such

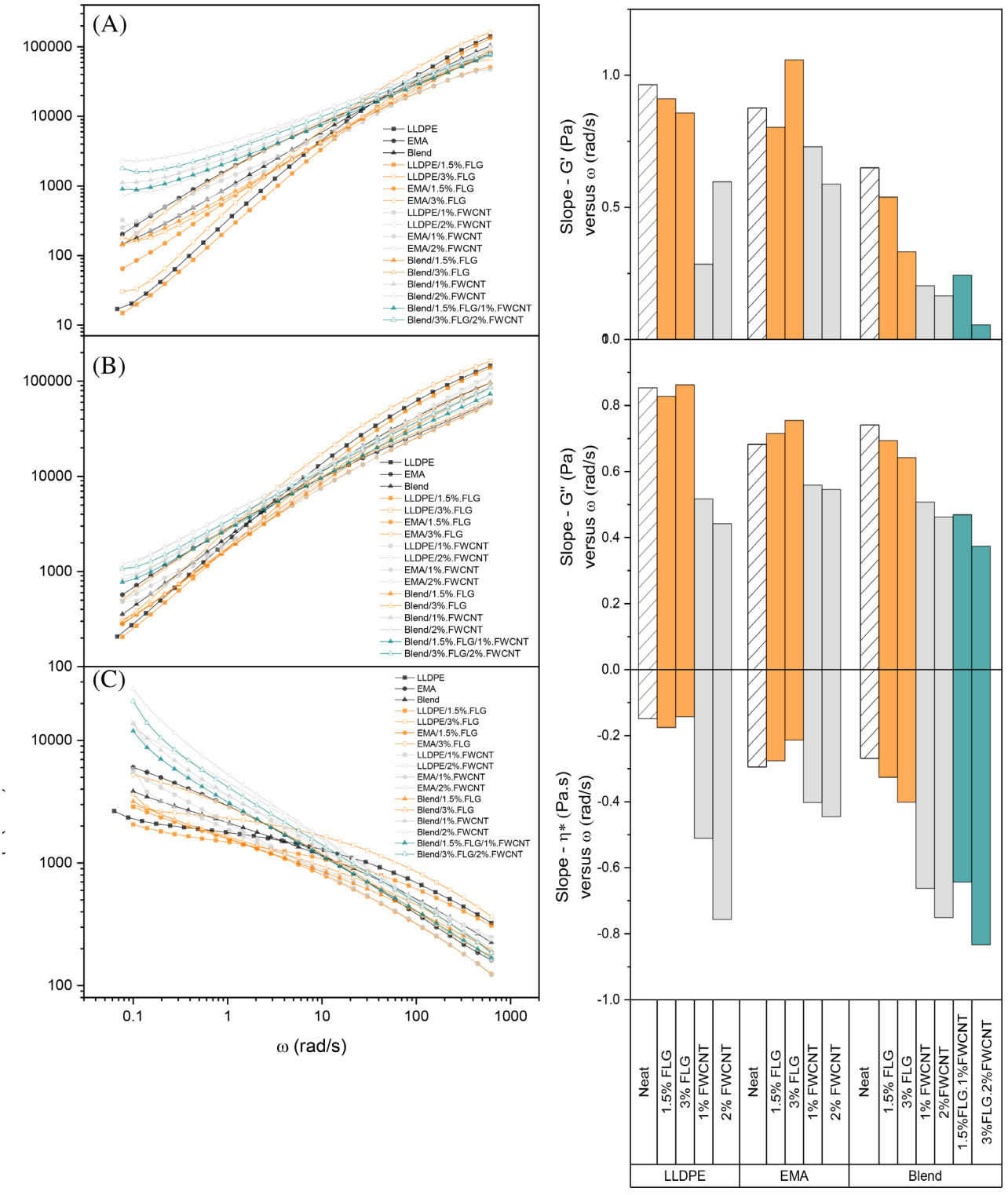

FIGURE 7 Plot of G' vs ω, A, G'' vs ω, B, η^* vs ω, C, tan δ vs ω, D, δ vs $|G^*|$, E, λ vs ω, F, for the linear low-density polyethylene (LLDPE), ethylene-*co*-methylacrylate (EMA), and LLDPE/EMA nanocomposites with few-layer graphene (FLG) and few-walled carbon nanotube (FWCNT) [Color figure can be viewed at wileyonlinelibrary.com]

compositions. Attempting to reaffirm the above considerations, the relaxation time was analyzed (λ), which can be calculated as follows[54]:

$$\lambda = \frac{G'}{\eta^* x\, \omega^2} \tag{11}$$

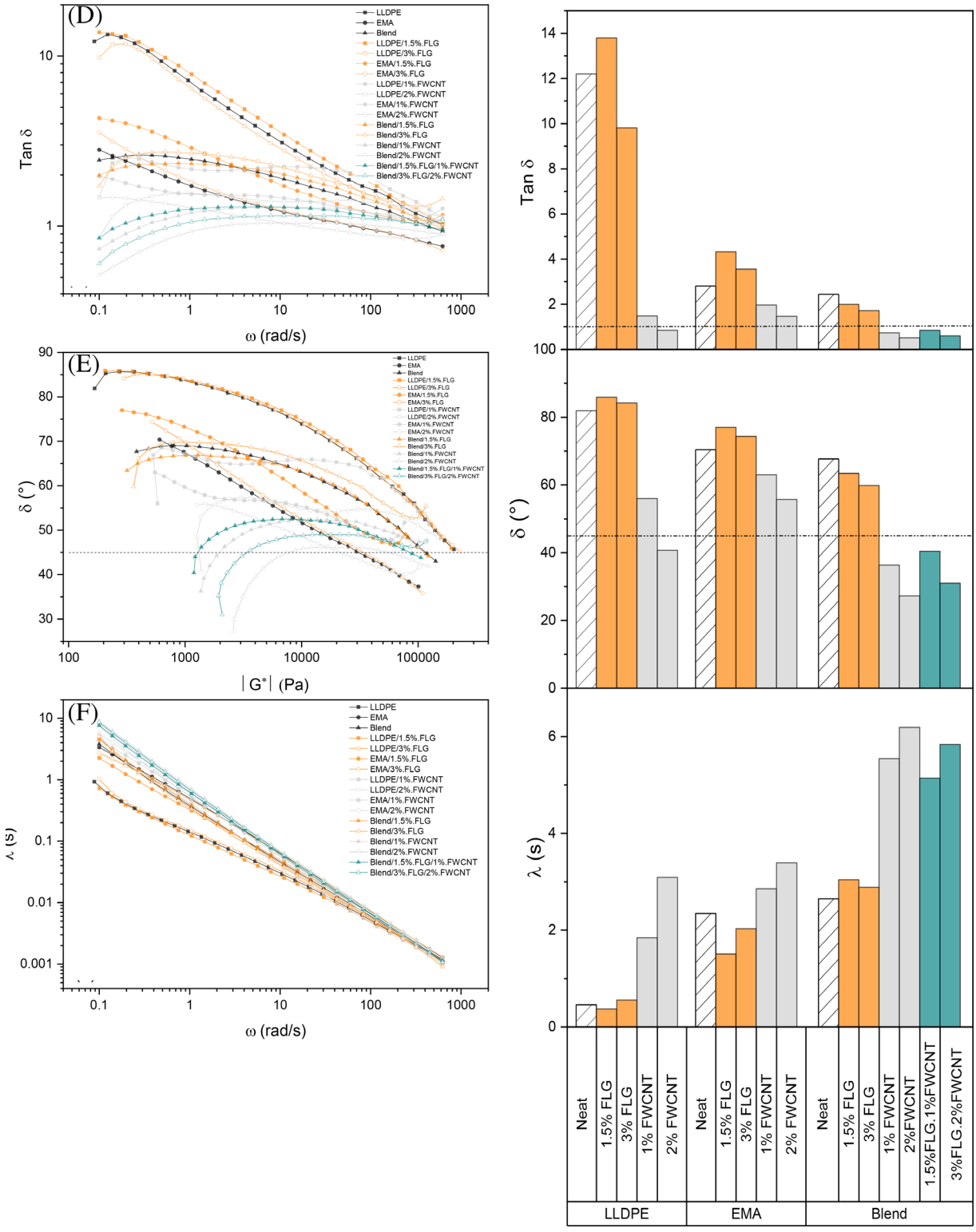

FIGURE 7 (Continued)

It is known that relaxation time represents the time required by the polymer molecules to relax completely during processing. It can indicate whether there is any in-built stress in the sample or not. If processing time is more significant than relaxation time, then the polymer molecules contain no in-built stress.[55] In Figure 7F, it can be observed that the relaxation time of the compositions with FWCNT and FLG/FWCNT is much longer than the neat polymers; compared to the nanocomposites with FLG that have a relaxation time near to the neat

polymers. This increase in the relaxation time can be related to the retaining of the polymer chains mobility due to the formation of a percolated network structure, which needs a longer time for breaking.[56]

5.6 | Electrical conductivity

Figure 8 shows the electrical conductivity of the compositions with LLDPE, EMA, and LLDPE/EMA as a function of the different mass fractions of FLG, FWCNT, and FLG/FWCNT. It can be observed that for almost all compositions (neat polymers and blends), there was an increase in the electrical conductivity proportional to the increase in the fraction of filler used: whether FLG or FWCNT. In this case, the percentage increase ranged from 10.7% (from 1% to 2% of FWCNT in LLDPE) to 66.2% (from 1.5% to 3% FLG in LLDPE).

Regarding the type of filler, for the compositions with one matrix, a significative difference was not observed. However, when the same comparison is made with LLDPE/1% FWCNT, and EMA/1% FWCNT samples, an increased range from 61.6% for LLDPE and 132.1% for EMA can be observed when compared to the LLDPE/1.5%FLG and EMA/1.5%FLG compositions, as shown in Figure 8. Since the electrical conductivities of the FLG and FWCNT nanofillers are equivalent,[57] the better dispersion of the FWCNT in the polymer matrix, is probably the main factor responsible for the better electrical conductivity observed in its nanocomposites (as presented Figure 7). This happens because rod-like structures are more effective than nanofillers of disc-like structures in creating conductive networks.[15] Besides, possible wrinkling, crimping, and scrolling can reduce the aspect ratio of the FLG. The factors mentioned above lead to the higher electrical conductivity of FWCNT-based nanocomposites in comparison with FLG-based nanocomposites for neat polymer compositions.[8]

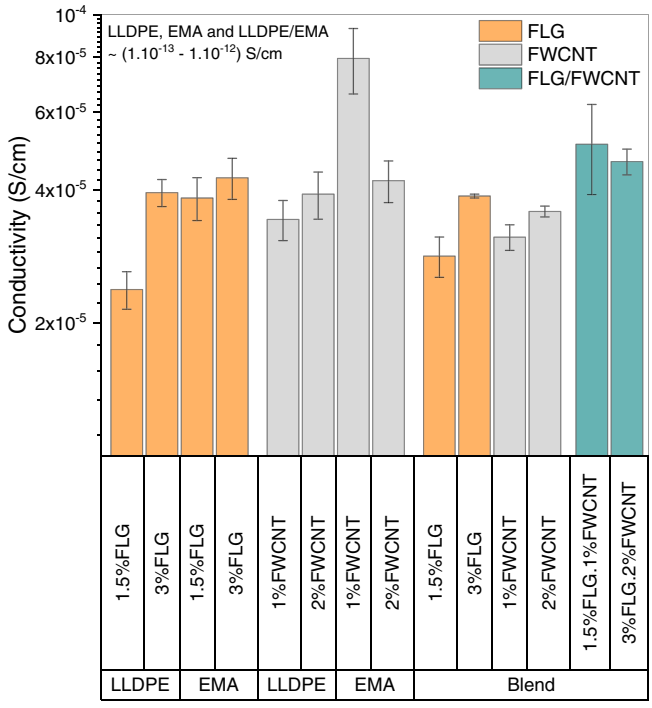

FIGURE 8 Electrical conductivity of the few-layer graphene (FLG), few-walled carbon nanotube (FWCNT), and FLG/FWCNT nanocomposites [Color figure can be viewed at wileyonlinelibrary.com]

It is important to note that during the manufacturing process of these nanocomposites, no surfactant was used for the dispersion of either nanotubes or graphene. Thus, the lower electrical conductivity improvement of the blends regarding the neat polymers may have been due to the presence of a layer of polymer between the nanofillers, interfering with the formation of a more efficient electrical conducting path, preventing the direct contact between the nanofillers and acting as an insulating layer in the tunneling barrier for electrical transport.[58] Furthermore, the extrusion was in two stages for the blends, which may have led to a reduction in the dimensions of the nanoparticles.

For the blends, although there was no significant improvement over the same compositions of neat polymers containing nanofillers, it was observed that the two hybrids studied (Blend/1.5%FLG/1%FWCNT and Blend/3%FLG/2%FWCNT) presented values of electrical conductivity higher than almost all the compositions evaluated (Figure 8). In the compositions containing only graphene or CNT, agglomeration or restacking may occur, respectively. In the case of hybrid polymer nanocomposites, the coexistence of CNTs and graphene may inhibit these interactions due to the increase of the steric hindrance through the π-π interactions of the CNTs and the graphene sheets due to the presence of CNTs between the graphene sheets. Another possible explanation for the best results observed for the FWCNT/FLG hybrid nanocomposites is the reduction in contact resistance due to the formation of 1D-2D interconnections, which increase the contact area, decreasing the electrical resistivity.[59]

5.7 | Comparison between rheological and electrical percolation

It is known that electrical and rheological percolation thresholds are dependent on the characteristics of the nanoparticles (size, type, and geometry), the polymer matrix (viscosity and molecular weight), and processing

conditions.[60] Before comparing these properties, it is important to clearly define the electrical and percolation threshold. The electrical percolation threshold is reached when a conductive path is formed across the material above the critical concentration of the conducting phase. The electrical conduction is described by two mechanisms: direct conduction (when there is direct contact between the fillers) or electron hopping (when the electrons "jump" from a conductive filler to another).[61] The rheological percolation threshold is a transition from liquid-like to solid-like behavior in the melt state, which is usually associated with an abrupt increase in their elasticity values due to the formation of a nanoparticle network through the matrix.[60]

It has been observed that in many of the literature studies using similar matrices,[62–67] the amount of graphene and CNT used in these studies ranges from 1.6 to 3.3 times higher than in the work presented in this article to achieve conductivity values up to 1000 times lower than those shown in Figure 8. As shown in Figure 8, the abrupt increase in the electron conductivity from 10^{-12} S/cm (nonmodified polymer matrix) to 10^{-5}-10^{-4} S/cm (nanocomposites), indicates a higher degree of connectivity within the embedded conducting phase, suggesting that electric percolation was attained. However, rheological percolation was only verified in five nanocomposites. An explanation lies in the absence of physical touching between the nanofillers.[63] For electrical percolation, this is not necessary due to the hopping/tunneling effect,[68] such a feature can result in a higher rheological threshold for these compositions. It is important to highlight that for the electrical conductivity range obtained in this work these films can be used for many engineering applications, such as electrically conducting adhesives, antistatic coatings and films, electromagnetic interference shielding materials for electronic devices, thermal interface materials, and so forth.[69]

6 | CONCLUSIONS

LLDPE/EMA/FLG/FWCNT hybrids nanocomposites were produced by the melt compounding technique, using a twin-screw extruder. As proposed initially, electrical conductivity was considerably improved for all the compositions evaluated. Below it is well explained the reasons for this achievement. Raman spectroscopy showed that despite the high shear rates presented in the extrusion process, the ratio values of the calculated I_D/I_G intensities for the nanocomposites with FLG and FWCNT showed that they maintained their structural quality with few defects. In addition, because the I_{2D}/I_G values were two times higher than those observed for FLG, it may be suggested that there was a reduction in the number of the graphene sheets during processing in the extruder. Analysis of the surface properties showed a better wettability between EMA-FLG and LLDPE-FWCNT. Scanning electron micrographs confirmed the predicted co-continuous morphology in the blend and a better dispersion in the blend containing FLG/FWCNT. The reduced values of the phase angle (<45°) and damping factor <1, for the LLDPE/EMA blends with FWCNT and for its hybrids with FLG/FWCNT, confirmed the rheological percolation of these compositions. This result agrees with the CA measurements, where the predominantly hydrophobic character of the LLDPE matrix, facilitated the dispersion of the FWCNT and consequently, the formation of a percolated network.

However, the hydrophilic character of the EMA may have contributed to the nonformation of a rheologically percolated network in the EMA compositions with the nanofillers. The electrical conductivity analyses showed that an increase of at least six orders of magnitude is observed for the nanocomposites compared to the unfilled polymers. By increasing the filler volume fraction, there was no noticeable difference between the conductivities within the nanocomposites with the same matrix, regardless of the type of filler used, suggesting that the percolation threshold was attained for a small volume fraction of the conducting component. However, in the hybrids, an improvement in this property was observed, corroborating the physical properties observed in the other characterizations.

ACKNOWLEDGMENTS

This research was supported by the Coordenação de Aperfeiçoamento de Pessoal de Nível Superior - Brasil (CAPES) - Finance Code 001 (scholarship granted to Mr Mário André Brito Seixas Nunes) and also by Conselho Nacional de Desenvolvimento Científico e Tecnológico (CNPq). G. J. M. F. acknowledges the financial support from FAPESP (grants 2018/10910-8) and CNPq (grant 307665/2018-6). T. J. A. M. acknowledges the financial support from CNPq (grant 306307/2019-7). Thanks also to Pankaj Agrawal for his assistance in training rheological tests.

ORCID

Tomás J. A. de Melo https://orcid.org/0000-0002-5879-6764

Guilhermino J. M. Fechine https://orcid.org/0000-0002-5520-8488

REFERENCES

[1] S. Y. Yang, W. N. Lin, Y. L. Huang, H. W. Tien, J. Y. Wang, C. Ma, C. C. Li, Y. S. Wang, *Carbon* **2011**, *49*, 793.

[2] S. Chatterjee, F. Nafezarefi, N. Tai, L. Schlagenhauf, F. Nüesch, B. Chu, *Carbon* **2012**, *50*, 5380.
[3] V. H. Pham, T. T. Dang, S. H. Hur, E. J. Kim, J. S. Chung, *ACS Appl. Mater. Interfaces* **2012**, *4*, 2630.
[4] H. Hu, G. Zhang, L. Xiao, H. Wang, Q. Zhang, Z. Zhao, *Carbon* **2012**, *50*, 4596.
[5] M. Li, C. Gao, H. Hu, Z. Zhao, *Carbon* **2013**, *65*, 371.
[6] J. Chen, X. Cui, Y. Zhu, W. Jiang, K. Sui, *Carbon* **2017**, *114*, 441.
[7] L. Bai, S. He, J. W. Fruehwirth, A. Stein, C. W. Macosko, X. J. Cheng, *J. Rheol.* **2017**, *61*, 575.
[8] M. H. Al-Saleh, *Synthetic Met.* **2015**, *209*, 41.
[9] M. Liebscher, M. O. Blais, P. Pötschke, G. Heinrich, *Polymer* **2013**, *54*, 5875.
[10] C. W. Lou, C. L. Huang, Y. J. Pan, Z. I. Lin, X. M. Song, J. H. Lin, *J. Polym. Res.* **2016**, *23*, 1.
[11] D. Yan, H. B. Zhang, Y. Jia, J. Hu, X. Y. Qi, Z. Zhang, Z. Z. Yu, *ACS Appl. Mater. Interfaces* **2012**, *4*, 4740.
[12] H. Qi, C. Qian, J. Liu, *Chem. Mater.* **2006**, *18*, 5691.
[13] X. Y. Fang, X. X. Yu, H. M. Zheng, H. B. Jin, L. Wang, M. S. Cao, *J. Phys. Lett. A* **2015**, *379*, 2245.
[14] A. R. Muñoz, C. F. Oliveira, L. G. Amurin, C. L. Rodriguez, D. A. Nagaoka, M. I. Tavares, S. H. Domingues, R. J. Andrade, G. J. M. Fechine, *Express Polym. Lett.* **2018**, *12*, 930.
[15] M. H. Al-Saleh, *Synthetic Met.* **2016**, *217*, 322.
[16] Y. J. Xiao, W. Y. Wang, X. J. Chen, T. Lin, Y. T. Zhang, J. H. Yang, Y. Wang, Z. W. Zhou, *Compos. Part A: Appl. Sci.* **2016**, *90*, 614.
[17] A. Das, G. R. Kasaliwal, R. Jurk, R. Boldt, D. Fischer, K. W. Stöckelhuber, G. Heinrich, *Compos. Sci. Technol.* **2012**, *72*, 1961.
[18] D. K. Owens, R. Wendt, *J. Appl. Polym. Sci.* **1969**, *13*, 1741.
[19] D. Kaelble, *J. Adhes.* **1970**, *2*, 66.
[20] F. M. Fowkes, *J. Ind. Eng. Chem.* **1964**, *56*, 40.
[21] K. Y. Law, H. Zhao, *Surface Wetting*, Springer, Switzerland **2016**, p. 135.
[22] B. D. Favis, *Polym. Blends* **2000**, *1*, 501.
[23] L. A. Utracki, *Commercial Polymer Blends*, Springer Science & Business Media, New York, NY **2013**.
[24] Y. Lan, H. Liu, X. Cao, S. Zhao, K. Dai, X. Yan, G. Zheng, C. Liu, C. Shen, Z. Guo, *Polymer* **2016**, *97*, 11.
[25] L. Li, Z. Wang, P. Zhao, Y. Luo, L. Liao, K. Xu, P. Li, Z. Wang, Z. Peng, *Eur. Polym. J.* **2017**, *92*, 275.
[26] Y. Pan, X. Liu, X. Hao, Z. Starý, D. W. Schubert, *Eur. Polym. J.* **2016**, *78*, 106.
[27] N. Mekhilef, H. Verhoogt, *Polymer* **1996**, *37*, 4069.
[28] L. A. Utracki, *J. Rheo.* **1991**, *35*, 1615.
[29] S. Steinmann, W. Gronski, C. Friedrich, *Polymer* **2001**, *42*, 6619.
[30] H. F. Giles, E. M. Mount, J. R. Wagner, *Extrusion: The Definitive Processing Guide and Handbook*, William Andrew, Norwich, NY **2004**.
[31] C. F. Oliveira, P. A. Muñoz, M. C. Santos, G. S. Medeiros, A. Simionato, D. A. Nagaoka, E. A. Souza, S. H. Domingues, G. J. M. Fechine, *Polym. Compos.* **2019**, *40*, E312.
[32] M. Bera, P. K. Maji, *Polymer* **2017**, *119*, 118.
[33] W. S. Kang, K. Y. Rhee, S. Park, *Compos. Part. B: Eng.* **2017**, *114*, 175.
[34] S. Prolongo, R. Moriche, A. J. Suárez, M. Sánchez, A. Ureña, *Eur. Polym. J.* **2014**, *61*, 206.
[35] R. Raj, S. C. Maroo, E. N. Wang, *Nano. Lett.* **2013**, *13*, 1509.
[36] D. W. Hoeppner. *Structural Integrity Considerations in Engineering Design*, Imperial College Press, London **2016**.
[37] M. Rashad, F. Pan, J. Zhang, M. Asif, *J. Alloy. Cmpd.* **2015**, *646*, 223.
[38] M. Giulianini, N. Motta, *Self-Assembly of Nanostructures*, Springer, New York, NY **2012**, p. 1.
[39] A. C. Ferrari, J. Meyer, V. Scardaci, C. Casiraghi, M. Lazzeri, F. Mauri, S. Piscanesc, D. Jiang, K. S. Novoselov, S. Roth, A. K. Geim, *Phys. Rev. Lett.* **2006**, *97*, 187401.
[40] J. Suh, D. Bae, *Compos. Part B: Eng.* **2016**, *95*, 317.
[41] L. M. Malard, M. Pimenta, G. Dresselhaus, M. Dresselhaus, *Phys. Rep.* **2009**, *473*(5–6), 51.
[42] D. G. Papageorgiou, I. A. Kinloch, R. J. Young, *Carbon* **2015**, *95*, 460.
[43] D. L. Silva, J. L. E. Campos, T. F. D. Fernandes, J. N. Rocha, L. R. P. Machado, E. M. Soares, D. R. Miquita, H. Miranda, C. Rabelo, O. P. V. Neto, A. Jorio, L. G. Cançado, *Carbon* **2020**, *161*, 181.
[44] A. A. Vasileiou, A. Docoslis, M. Kontopoulou, P. Xiang, Z. J. P. Ye, *Polymer* **2013**, *54*, 5230.
[45] J. N. Coleman, U. Khan, W. J. Blau, Y. K. Gun'ko, *Carbon* **2006**, *44*, 1624.
[46] C. A. Cooper, R. Young, M. Halsall, *Comp. Part A: Appl. Sci.* **2001**, *32*, 401.
[47] E. F. Antunes, A. Lobo, E. Corat, V. T. Airoldi, *Carbon* **2007**, *45*, 913.
[48] P. Pötschke, D. Paul, *J. Macromol. Sci. Polym. Rev.* **2003**, *43*, 87.
[49] U. Niebergall, J. Bohse, B. Schürmann, S. Seidler, W. Grellmann, *Polym. Eng. Sci.* **1999**, *39*, 1109.
[50] T. W. Lee, Y. G. Jeong, *Compos. Sci. Technol.* **2014**, *103*, 78.
[51] Y. C. Chiu, C. L. Huang, C. Wang, *Compos. Sci. Technol.* **2016**, *134*, 153.
[52] S. S. Chauhan, M. Verma, P. Verma, V. P. Singh, V. Choudhary, *Polym. Adv. Technol.* **2018**, *29*, 347.
[53] T. Gong, M. Q. Liu, H. Liu, S. P. Peng, T. Li, R. Y. Bao, W. Yang, B. H. Xie, M. B. Yang, Z. Guo, *Polymer* **2017**, *110*, 1.
[54] D. Wu, L. Wu, M. Zhang, Y. Zhao, *Polym. Degrad. Stabil.* **2008**, *93*, 1577.
[55] S. Basu, M. Singhi, B. K. Satapathy, M. Fahim, *Polym. Compos.* **2013**, *34*, 2082.
[56] Y. Zare, K. Y. Rhee, *Compos. B: Eng.* **2019**, *156*, 100.
[57] J. Du, L. Zhao, Y. Zeng, L. Zhang, F. Li, P. Liu, C. Liu, *Carbon* **2011**, *49*, 1094.
[58] S. Paszkiewicz, A. Szymczyk, D. Pawlikowska, J. Subocz, M. Zenker, R. Masztak, *Nanomaterials* **2018**, *8*, 264.
[59] J. Y. Oh, G. H. Jun, S. Jin, H. J. Ryu, S. H. Hong, *ACS Appl. Mater. Interfaces* **2016**, *8*, 3319.
[60] A. Zohrevand, A. Ajji, F. Mighri, *Rheol. Acta* **2014**, *53*, 235.
[61] C. Penu, G. H. Hu, A. Fernandez, P. Marchal, L. Choplin, *Polym. Eng. Sci.* **2012**, *52*, 2173.
[62] M. Sabet, H. Soleimani, *IOP Conf. Ser. Mater. Sci. Eng.* **2014**, *64*, 012001.
[63] R. Socher, B. Krause, M. T. Müller, R. Boldt, P. Pötschke, *Polymer* **2012**, *53*, 495.
[64] P. K. Rajamani, R. Boros, *Acta Tech. Jaurinensis* **2018**, *11*, 185.

[65] G. Santagiuliana, *Preparation, Characterisation, and Modelling of Graphene-based Polymer Nanocomposites with Enhanced Mechanical and Electrical Properties*, Queen Mary University of London, London **2019**.

[66] G. Georgousis, I. Charitos, E. Kontou, S. Koutsoumpis, Z. Terzopoulou, D. Bikiaris, *Polym. Compos.* **2018**, *39*, E1118.

[67] M. Sabet, H. Soleimani, E. Mohammadian, *J. Vinyl Addit. Technol.* **2019**, *25*, 35.

[68] M. Chapartegui, N. Markaide, S. Florez, C. Elizetxea, M. Fernandez, A. Santamaría, *Compos. Sci. Technol.* **2010**, *70*, 879.

[69] P. C. Ma, N. A. Siddiqui, G. Marom, J. K. Kim, *Compos. Part A: Appl. Sci. Manuf.* **2010**, *41*, 1345.

How to cite this article: Nunes MABS, de Matos BR, Silva GG, Ito EN, de Melo TJA, Fechine GJM. Hybrids nanocomposites based on a polymer blend (linear low-density polyethylene/poly(ethylene-*co*-methyl acrylate) and carbonaceous fillers (graphene and carbon nanotube). *Polymer Composites*. 2021;42:661–677. https://doi.org/10.1002/pc.25856